Value of Bulk Heat Flux Parameterizations for Ocean SST Prediction

ALAN J. WALLCRAFT, A. BIROL KARA, HARLEY E. HURLBURT, AND E. JOSEPH METZGER

Oceanography Division, Naval Research Laboratory, Stennis Space Center, MS

ERIC P. CHASSIGNET AND GEORGE H. HALLIWELL

Rosenstiel School of Marine and Atmospheric Science, University of Miami, FL

Corresponding author address: Birol Kara: Naval Research Laboratory, Code 7320, Bldg. 1009,

Stennis Space Center, MS 39529–5004, USA.

E–mail: Birol.Kara@nrlssc.navy.mil

ABSTRACT

Bulk heat flux parameterization is an increasingly popular technique for forcing non–coupled ocean models. If sea surface temperature (SST) from the model is colder (warmer) than observed, then the net heat flux will be higher (lower) than observed; thus, bulk parameterizations tend to keep model SST close to observational SST on long time scales. However, bulk parameterizations imply neither strong damping of SST variability nor strong relaxation to near–surface (e.g., at 10 m) air temperature (T_a). This is demonstrated using SST simulations from a $0.72° \times 0.72°$ cos(lat) (longitude $\times$ latitude) resolution global HYbrid Coordinate Ocean Model (HYCOM) that does not include assimilation of any SST data or explicit relaxation to any SST climatology, but does use bulk heat fluxes. Results are discussed when climatological wind and thermal atmospheric forcing for HYCOM are constructed from three different archived numerical weather prediction (NWP) products: (1) the European Centre for Medium–Range Weather Forecasts (ECMWF) 15–year Re–Analysis during 1979–1993 (ERA–15), (2) ECMWF 40–year Re–Analysis (ERA–40) during 1979–2002, and (3) the Common Ocean Reference Experiment Corrected Normal Year forcing version 1.0 (CORE–CNY) based on the National Center Environmental (NCEP) re–analysis which spans 1948–2002. To investigate the implications of the bulk heat flux approach as relaxation to SST and T_a, HYCOM SST simulations are used to demonstrate that model SST errors with respect to the National Oceanic Atmospheric Administration (NOAA) SST climatology do not look like T_a–SST fields from NWP products. Such a result is confirmed for all simulations forced with ERA–15, ERA–40 and CORE–CNY, separately. Overall, global averages of mean HYCOM SST error are $0.23°$C ($1.54°$C), $0.42°$C ($1.73°$C) and $0.57°$C ($2.32°$C) with respect to NOAA SST (NWP T_a) climatology when the model uses atmospheric forcing from ERA–15, ERA–40 and CORE–CNY, respectively.

1. Introduction and motivation

Ocean general circulation model (OGCM) simulations are generally performed using prescribed atmospheric forcing fields, namely, momentum flux (e.g., wind stress) and scalar forcing (e.g., net shortwave and longwave radiation at the sea surface, air temperature and air mixing ratio at 10 m above the sea surface). These forcing fields are typically obtained from archived NWP products. Examples of commonly–used NWP products include the European Centre for Medium–Range Weather Forecasts (ECMWF) 15–year Re–Analysis (ERA–15) (Gibson et al. 1999), ECMWF 40–year Re–Analysis (ERA–40) (Kållberg et al. 2004), National Centers for Environmental Prediction (NCEP) Re–Analysis (Kalnay et al. 1996; Kanamitsu et al. 2002), and the Fleet Numerical Meteorology and Oceanography Center (FNMOC) Navy Operational Global Atmospheric Prediction System (NOGAPS) (Rosmond et al. 2002).

All NWPs mentioned above use relatively sophisticated boundary layer sub–models to calculate surface fluxes, but they still depend on SST which is usually an analyzed (non–prognostic) field. The SST used is now accurate enough that errors in surface fluxes at the NWP grid–scale are dominated by errors in atmospheric fields, such as wind speed and cloudiness. These errors can be large, and even the best surface heat flux fields from all sources (NWP products or observation–based climatologies) do not give a closed global heat budget. In addition, using climatological estimates of total heat flux to force an ocean model usually results in unrealistic model SST, presenting an inconsistency with the imposed surface flux (Barnier et al. 1995).

Even perfect fluxes, with a closed global heat budget, cannot be used as the only forcing for a stand–alone ocean model because the model's "climatology" is not perfect, so such fluxes will lead to SST drift (e.g., Moore and Reason 1993; Hughes and Weaver 1996). The conventional approach to correcting this drift is to add relaxation to observed SST, either in place of, or in addition to, prescribed total heat fluxes (e.g., Barnier et

al. 1995, Maltrud et al. 1998). As stated by Killworth (2000), researchers at this time did not possess consistent surface fields with which to force their models. However, the use of a bulk parameterization has become an alternative approach because it requires no explicit relaxation to observed oceanic quantities (e.g., Wallcraft et al. 2003; Kara et al. 2003).

Bulk parameterizations use the difference T_a–SST, where T_a is the air temperature and SST the ocean model sea surface temperature. The air temperature and other parameters (air density at the air–sea interface, mixing ratio, and wind speed at 10 m above the sea surface) are typically from NWP products and are used to calculate the exchange coefficients for latent and sensible heat fluxes (e.g., Kara et al. 2002). The most important criticisms of bulk parameterizations are that (1) an infinite heat capacity exists between ocean and atmosphere, i.e., it does not give a closed system, and (2) since the bulk formula can be linearized as a function of a difference between equilibrium temperature and SST (Haney 1971; Han 1984; Paiva and Chassignet 2001), it can smear the model SST when the model resolution is finer than the forcing.

In this paper, we examine the impact of bulk heat flux parameterization on the climatological SST produced by simulations from a particular global OGCM, with no assimilation of or explicit relaxation to any observed SST climatology. In particular, reasons for preferring the bulk parameterization rather the net heat flux plus an explicit relaxation to SST are discussed.

A few salient reasons for using SST from an OGCM to discuss the bulk heat flux versus the direct relaxation approach are (1) SST plays an important role in air–sea interactions through the net heat flux at the sea surface (e.g., Alexander and Scott 1997); (2) it is typically used in the bulk heat flux formulation to parameterize the stability (Kara et al. 2000); (3) it plays a major role in controlling long term climate variations, such as the North Atlantic Oscillation (Paeth et al. 2003); (4) it is one of the best observed variables of the

3

upper ocean over the global ocean; therefore, SSTs simulated from an OGCM can be easily validated over the globe (Schopf and Loughe 1995). In addition, SST from an atmospherically–forced OGCM (no assimilation of any ocean data, including SST) is used because one of our goals is to demonstrate that, although the bulk heat flux formulation forcing an OGCM surface temperature field includes the knowledge of air temperature near the sea surface, such use does not imply an improper form of SST restoring within the model.

The paper is organized as follows. Section 2 discusses the tradiational bulk heat flux approach for OGCMs. Section 3 gives details of the OGCM used in this study. Section 4 presents SST results from an OGCM in relation to the bulk heat flux parameterization, and section 5 gives conclusions of this paper.

2. Bulk Heat Flux Approach

The total heat flux (Q_{net}) at the sea surface can be expressed as follows:

$$Q_{\text{net}} = Q_{\text{sw}} - Q_{\text{lw}} + Q_l + Q_s, \tag{1}$$

where Q_{sw} is the net shortwave radiation at the sea surface, Q_{lw} is the net longwave radiation at the sea surface, Q_l is the latent heat flux, and Q_s is the sensible heat flux.

All these individual components, and their total, Q_{net}, are typically available from the archived real–time and re–analysis data sets or from climatologies (ERA–15, ERA–40 and CORE–CNY are used here). Shortwave, Q_{sw}, and longwave, Q_{lw}, radiation can be directly measured at the surface, but there are far too few such observations to constrain even regional fluxes. Thus, in practice all components are estimated. All components are affected by surface type i.e., land versus sea versus sea–ice (Garratt et al. 1998), but here we will only consider the open ocean. Both shortwave and longwave radiation depend heavily on cloudiness, and all flux components except shortwave radiation depend on SST (e.g., Gill 1982; Gleckler and Weare 1997). HYCOM uses a penetrating solar radiation scheme (Kara et al. 2005a) that accounts for spatial and temporal

water turbidity (Kara et al. 2005b,c).

While SST drift in OGCMs may be significantly reduced by relaxation to observed SST (e.g., Barnier et al. 1995), such an approach has the important shortcoming that the correct result is prescribed in the model simulation. Rather than using a direct SST relaxation scheme, an alternative approach is to calculate fluxes from a bulk parameterization based on near–surface atmospheric fields using only near–surface wind speed ($\mathbf{v}_a$) as presented in Large and Pond (1981), or also including air mixing ratio (q_a), near–surface air temperature (T_a) (all of which are 10 m above the sea surface), mixing ratio for sea water (q_s) and model SST, as explained in Kara et al. (2005d).

Bulk parameterizations are based on statistical fits to observations. They are usually inexpensive to calculate, and the best parameterizations are generally very accurate. Examples of typical bulk parameterizations for latent and sensible heat fluxes can be found in DeCosmo et al. (1996), Kara et al. (2000, 2002), and Fairall et al. (2003). The formulation used in HYCOM is briefly described as follows:

$$Q_s \;\; = \;\; C_s\, C_p\, \rho_a\, \mathbf{v}_a\, (T_a - SST) \tag{2}$$

$$Q_l \;\; = \;\; C_l\, L\, \rho_a\, \mathbf{v}_a\, (q_a - q_s) \tag{3}$$

The air density at the air–sea interface (ρ_a) in kg m^{-3} is determined using the ideal gas law. The exchange coefficients (C_l and C_s) used in HYCOM include the effects of boundary layer stability, and are expressed as polynomial functions of T_a–SST, $\mathbf{v}_a$, and $q_a - q_s$, the latter through relative humidity (RH), where RH is at the air–sea interface (see http://www7320.nrlssc.navy.mil/nasec/nasec.html). In the polynomial functions, the effects of water vapor flux in calculating the exchange coefficients are taken into account through RH effects that are especially important at low wind speeds (Kara et al. 2005d). The total heat flux (Eq. 1) is therefore

5

expressed as a polynomial function of the model SST and can be linearized to first order as

$$Q_{\mathrm{net}} = \lambda(T^* - \mathrm{SST}), \qquad (4)$$

in which the apparent equilibrium temperature T^* and the relaxation coefficient λ are time and space dependent and can be computed from the atmospheric fields (Haney 1971; Han 1984; Paiva and Chassignet 2001). We have included Q_{sw} in the Haney parameterization, as is usually done, even though it does not depend on SST. The total heat flux therefore implies a temperature relaxation, but not toward the atmospheric temperature T_a, nor toward a "correct" SST (T_c). The equilibrium temperature T^* indeed must differ from the "correct" SST (T_c) as it would otherwise imply zero heat flux when the model SST is equal to T_c. Overall, the resulting model SST is the result of a delicate balance between advection, vertical and horizontal mixing, and direct forcing. For the model SST to be near T_c, one therefore not only needs a good bulk parameterization of the heat flux, but also correct ocean model velocity fields and good mixed layer physics. An investigation of model SST accuracy in comparison to observations is therefore not only a test of the bulk formula, but also of the model physics and dynamics.

As mentioned in the introduction, a common alternative has been to use NWP net flux plus an explicit relaxation to the correct SST, T_c. Since SST is one of the best observed geophysical fields, why should a bulk parameterization be preferred over the NWP net flux plus an explicit relaxation to SST? One answer is that the e–folding time implicit in accurate bulk parameterizations is representative of the air–sea interface. It is possible to construct explicit relaxation terms that are patterned on bulk parameterizations, or alternatively to use measured climatological e–folding times from observations or NWP fields (or the results of a bulk parameterization applied to NWP fields). These approaches are all of the Haney type (Haney 1971; Han 1984,

da Silva et al. 1994, Paiva and Chassignet 2001) and are obtained by expressing Eq. 4 as

$$Q(SST) \quad = \quad Q(T_c) + \frac{\partial Q}{\partial T}|_{T_c}(T_c - \mathrm{SST}), \tag{5}$$

where the effective SST relaxation e–folding time scale implied by $\frac{\partial Q}{\partial T}|_{T_c}$ depends on many factors. However, it

is certainly positive and typically large enough that model SST does not exhibit long–term drift. In practice

relaxation terms are often simpler than this, i.e., a constant e–folding time.

Eddy–resolving, atmospherically–forced ocean models without ocean data assimilatio should not relax

strongly to synoptic observed SST because the observed SST will include SST anomalies associated with eddies

and western boundary currents at different locations than in the model simulation. This is because of flow

instabilities in the model which are not a deterministic response to the forcing. The bulk parameterization

does not use the NWP SST explicitly, and the NWP fields are often on a much coarser grid than the ocean

model one that barely resolves such details as eddy and ocean current locations. However, this raises the

question of to what degree the implied relaxation in the heat flux can smear the model SST when the model

resolution is finer than the forcing. It also raises the question as to whether the atmospheric temperature T_a is

strongly correlated to the NWP SST, therefore introducing oceanic information in the heat flux formulation. In

contrast, eddy–resolving stand–alone ocean models that assimilate sea surface height (from satellite altimeters)

have ocean fronts and eddies in the observed location (Smedstad et al. 2003; Chassignet et al. 2006; Shriver et

al. 2006) and therefore can relax directly to high resolution observed SST, although they may instead (or in

addition) directly assimilate SST. From the preceding discussion, simple relaxation is never appropriate as the

only heat flux term, so it must be augmented either with the NWP net heat flux or a bulk parameterization

heat flux.

Regions where the ocean model's mean SSTs are less accurate can often be traced to deficiencies in the

atmospheric fields. In particular, systematic biases in wind speed will always lead to poor fluxes from the bulk parameterization and biases in cloudiness will have a large effect on shortwave radiation (partially offset by changes to downward longwave radiation). Biased winds are unlikely to provide better surface heat fluxes from the sophisticated boundary layer sub–model in the NWP than from the bulk parameterization. Assimilation of wind speeds from satellites should improve the accuracy of NWP surface winds, but there are still large biases in some coastal regions, and there may be smaller systematic biases on larger scales. Cloud cover is difficult to obtain accurately, and known to be deficient regionally in both archived real time and re–analysis products.

In order to answer the question as to whether the atmospheric temperature, T_a, is strongly correlated to the SST, therefore introducing oceanic information into the heat flux formulation, the long term (climatological) mean of the difference between near–surface T_a and SST from an observation–based data set and the SST used by NWP products are investigated over the global ocean (Fig. 2). Specifically, the observation-based data set is the Comprehensive Ocean Atmosphere Data Set (COADS) climatology based largely on ship observations and buoy measurements during 1945–1989 (da Silva et al. 1997) and the NWP data products are the re–analysis products, ERA–15 (1979–1993), ERA–40 (1979–2002) and CORE–CNY (1948–2002). COADS is the only observation–based climatology among these products, and is intended to complement the comparisons. This is the new $1/2° \times 1/2°$ climatology based on the atlas of surface marine data, Supplement B (http://www.nodc.noaa.gov/OC5/asmdnew.html). Note that hereinafter the COADS SST and the SST analyses used in the NWP products will be denoted as T_s.

Although the time periods over which each climatology (COADS, ERA–15, ERA–40 and NCEP) is constructed are different, they are all ≥ 15 years which is adequate to represent a long term mean over the global ocean. Near–surface T_a and T_s data for each product are available from the National Center Atmospheric

Research (NCAR) web site (available online at http://dss.ucar.edu/catalogs/). COADS provides monthly mean T_a–T_s fields directly, while for the three NWP products we form climatological means using T_a and the T_s fields archived at sub–daily intervals. Near–surface atmospheric temperature T_a from ERA–15, ERA–40 and NCEP is at 2 m, while that from COADS is at 10 m above the sea surface. The adjustment from 2 to 10 m T_a is very small as indicated by the comparison of T_a values in Table 1 and hence was ignored.

When sea–ice is present, surface T_a is over sea–ice in the re–analysis products, but not in COADS. The T_a field from NCEP/NCAR is actually obtained from the CORE–CNY (Corrected Normal Year) data set which corrected for excessively cold values in the Antarctic. Ignoring high latitudes where sea–ice forms, the fields are broadly similar to each other with climatological T_s warmer than T_a nearly everywhere but usually by $\leq 1°$C. The exception is in areas where strong currents transport water which is significantly warmer than the air in the mean, e.g., Gulf Stream, Kuroshio and Agulhas.

The same long term mean fields shown in Fig. 2 are plotted as scatter diagrams of T_a vs $T_a - T_s$ over the global ocean (Fig. 3). The regions where ice is located is excluded when evaluating $T_a - T_s$ in the plots. There is a strong linear relationship between T_a and SST with R values > 0.99 for all data sets. This is clearly evident from the slope values being close to 1 in all cases (1.008, 0.991, 1.012 and 1.033 for COADS, ERA–15, ERA–40 and CORE–CNY, respectively). Intercept values are also similar with values of 0.468, 0.911, 0.711 and 0.405. The bias between T_a and T_s (i.e., $T_a - T_s$) ranges from $-0.64°$C for COADS to $-1.09°$C for CORE–CNY (Table 1).

In contrast, near–surface T_a and $T_a - T_s$ are only weakly correlated (Fig. 4) with linear correlation coefficients of –0.12, –0.14, –0.17 and –0.25 for COADS, ERA–15, ERA–40 and CORE–CNY. None of the correlation values are statistically significant in comparison to a correlation value of 0 at a 95% confidence

interval based on the student's t–test.

3. HYCOM description

The HYbrid Coordinate Ocean Model (HYCOM) is based on a primitive–equation formulation discussed by Bleck (2002), in detail. There have been several HYCOM applications investigating a variety of processes in different ocean basins and enclosed seas. Examples of such studies include the North Atlantic (Chassignet et al. 2003; Halliwell 2004; Thacker et al. 2004), the Indian Ocean (Han et al. 2005), the tropical Pacific (Shaji et al. 2005), and the Black Sea (Kara et al. 2005a,b,c). HYCOM has also been used as the ocean component of a coupled atmosphere–ocean model in global climate studies (e.g., Sun and Hansen 2003; Bleck and Sun 2004), and for eddy resolving ocean prediction (Chassignet et al. 2006).

For the present study, we will introduce HYCOM configured for the global ocean, including the latest advances in the model development (see appendix for details). The model presented here is a stand–alone ocean model with no assimilation of any ocean data, including SST, and no relaxation to any other data except sea surface salinity (SSS) to keep the evaporation minus precipitation balance on track. General features of the global atmospherically–forced HYCOM are given in section 3a and the atmospheric forcing used in the model simulations is explained in section 3b.

3a. General Features of global HYCOM

HYCOM contains five prognostic equations: two for the horizontal velocity components, a mass continuity or layer thickness tendency equation and two conservation equations for a pair of thermodynamic variables, such as salt and potential temperature or salt and potential density (Bleck 2002). The model behaves like a conventional σ (terrain–following) model in very shallow oceanic regions, like a z–level (fixed–depth) coordinate model in the mixed layer or other unstratified regions, and like an isopycnic–coordinate model in stratified

10

regions. However, the model is not limited to these coordinate types (Chassignet et al. 2003). Typically, HYCOM has isopycnal coordinates in the stratified ocean but uses the layered continuity equation to make a dynamically smooth transition to z–levels in the unstratified surface mixed layer and σ–levels in shallow water. The optimal coordinate is chosen every time step using a hybrid coordinate generator. Thus, the model automatically generates the lighter isopycnal layers needed for the pycnocline during summer, but during winter the same layers define fixed–depth z–level coordinates.

HYCOM as used in this paper spans the global ocean from 78°S to 90°N (Fig. 1). It has a 0.72° equatorial Mercator grid between 78°S–47°N, with an Arctic bi–polar patch above 47°N. Average zonal (longitudinal) grid resolution for the 0.72° global model varies from $\approx$ 80 km at the equator to $\approx$ 60 km at mid–latitudes (e.g., at 40°N). The meridional (latitudinal) grid resolution is doubled near the equator to better resolve the equatorial wave–quide and halved in the Antarctic for computational efficiency. Hereinafter, the model resolution will be referred to as 0.72° for simplicity. Zonal and meridional array lengths are 500 and 457, respectively. At this resolution, coastal regions are not represented in great detail (so sigma–levels are not used), and the model land–sea boundary is at the 50 m isobath (with a closed Bering Strait).

All global simulations use sigma0 (sigma–theta), i.e. potential density referenced to the surface (0 dbar) with no thermobaric correction. There are 26 hybrid layers in the vertical. In general, the model needs fewer vertical coordinate surfaces than, say, a conventional z–level model, because isopycnals are more efficient in representing the stratified ocean, as discussed in Hurlburt et al. (1996) and Kara et al. (2005a). The target density values for the isopycnals and the decreasing change in density with depth between isopycnal coordinate surfaces are based on the 1/4° Generalized Digital Environmental Model (GDEM) climatology (NAVOCEANO 2003). The density difference values were chosen so that the layers tend to become thicker

11

with increasing depth, with the lowest abyssal layer being the thickest. The near–surface z–level regime is a natural consequence of HYCOM's minimum layer thickness. In this case, the minimum thickness of layer 1 is 3 m, and this minimum increases $1.125\times$ per layer up to a maximum at 12 m, and target densities are chosen, such that at least the top four layers are in z–level coordinates.

Monthly mean temperature and salinity from the GDEM climatology in August are used to initialize the model. The simulations use realistic bottom topography constructed from the NRL 2 minute resolution bathymetry. Extensive quality control of bottom topography was performed in straits and near coastlines. There is a relaxation to monthly mean SSS from the Polar science center Hydrographic Climatology (PHC). The PHC climatology is chosen for its accuracy in the Arctic region (Steele et al. 2001). The reference mixed layer thickness for the SSS relaxation is 30 m (30 days in 30 m e–folding time). The actual e–folding time depends on the mixed layer depth (MLD) and is $30 \times 30/\text{MLD}$ days, i.e. it is more rapid when the MLD is shallow and less so when it is deep. Such a relaxation is necessary to prevent SSS drift, and is in addition to the evaporation–precipitation budget.

HYCOM has several mixed layer/vertical mixing options (see Halliwell (2004) for a discussion and evaluation). In this paper, the non–slab K–Profile Parameterization (KPP) of Large et al. (1997) is used.

2b. Atmospheric Forcing

The model reads in the following time–varying atmospheric forcing fields: wind forcing (zonal and meridional components of wind stress, wind speed at 10 m above the sea surface) and thermal forcing (air temperature and air mixing ratio at 10 m above the sea surface, precipitation, net shortwave radiation and net longwave radiation at the sea surface). The wind/thermal forcing was constructed from three NWP products: (i) $1.125° \times 1.125°$ ERA–15, (ii) $1.125° \times 1.125°$ ERA–40 and (iii) $1.875° \times 1.875°$ CORE–CNY. A brief description

12

of each product is provided here.

The original atmospheric forcing data set from ERA–15 spans the period 1 January 1979–31 December 1993. The climatological ERA–15 forcing used here consists of 15–year monthly averages over 1979–1993, interpolated in time to 6 hourly and with 6 hourly sub–monthly anomalies from operational ECMWF in September 1994 to September 1995 added to the winds only. Choosing another time period for the 6 hourly wind anomalies (other than 1994–95) did not make any significant impact on the model SST. ECMWF used a spectral model to generate the ERA-15 dataset. The ERA-15 Re-analysis project incorporated a number of in situ and satellite–based data types over the 15–year period. Sea surface temperature analyses for ERA-15 are provided by the United Kingdom Meteorological Office (UKMO) for the early period, and by NOAA from November 1981 onwards. Sea ice cover has been derived from satellite data.

The ERA-40 project applies a modern variational data assimilation technique for the past conventional and satellite observations. The model physics and the surface parameterization have been upgraded and improved since ERA-15. A significant difference between ERA–40 and ERA–15 is in the use of satellite data. ERA–40 uses the Advanced Tiros Operational Vertical Sounde (ATOVS) radiances directly, while in ERA–15 temperature and humidity retrievals were used. In addition, Special Sensor Microwave Imager (SSM/I) and European Remote Sensing Satellite (ERS) data are used in ERA–40. The SST/Ice data set produced by the Hadley Centre and National Oceanic and Atmospheric Administration (NOAA)/National Environmental Satellite, Data, and Information Service (NESDIS) has been made available to the ERA–40 project. To support longer time period (1957–2002) covered by the ERA–40 project, ECMWF obtained a comprehensive archive of past observations from the National Centers for Environmental Prediction (NCEP) to supplement its original observational archives. For use in the analyses and model simulations performed here, 25–year monthly

13

climatologies of various parameters were formed from the ERA–40 archives spanning 1979–2002 with the same 6 hourly wind anomalies added as in the ERA–15 case.

The atmospheric forcing from CORE–CNY was introduced in Large and Yeager (2004), in detail; therefore details are not given here. This data set combines re–analysis data from NCEP with satellite measurements to reduce errors existing in the original NCEP fields, especially radiation fields (e.g., Lee et al. 2005). Heat fluxes for the CORE–CNY forcing are produced using NOAA SSTs and the NCAR bulk formulae. The forcing includes 6 hourly representative variability in all its fields. In each case, the intent is to include high temporal variability in the forcing, while maintaining a climatology.

In addition to wind and thermal forcing, HYCOM forcing incorporates monthly mean climatologies of river discharge and satellite–based attenuation coefficients for Photosynthetically Active Radiation (k_{PAR} in m^{-1}). The shortwave radiation at depth is calculated using a spatially and temporally varying monthly k_{PAR} climatology as processed from the daily–averaged k_{490} (attenuation coefficient at 490 nm) data set from Sea–viewing Wide Field–of–view Sensor (SeaWiFS) during 1997–2001. Thus, using ocean color data, the effects of water turbidity are included in the model simulations through the attenuation depth (k_{PAR}^{-1} in m) for shortwave radiation. The rate of heating/cooling of model layers in the upper ocean is obtained from the net heat flux absorbed from the sea surface down to a depth, including water turbidity effects (e.g., Kara et al. 2005a). Previously, it was shown that water turbidity can be quite significant in SST simulations, especially in equatorial regions (e.g., Kara et al. 2004; 2005b).

HYCOM treats rivers as a "runoff" addition to the surface precipitation field. The flow is first applied to a single ocean grid point and smoothed over surrounding ocean grid points, yielding a contribution to precipitation in $\mathrm{m\ s}^{-1}$. This works independently of any other surface salinity forcing. Monthly mean river

discharge values are taken from the NRL river climatology (Barron and Smedstad 2002). The hypothesis used in constructing the global river data set proposes that a database of monthly mean river discharges will be superior to a database of annual means in its ability to estimate real time discharge, and therefore it is preferred in this study. The NRL river data set comes from Perry et al. (1996) which had one mean value for each river but the set was converted to monthly values for use in ocean modeling studies as explained in Barron and Smedstad (2002).

The net surface heat flux that has been absorbed (or lost) by the upper ocean to depth is parameterized as the sum of the downward surface solar radiance, upward longwave radiation, and the downward latent and sensible heat fluxes (see section 3). Net solar radiation (the sum of net shortwave and longwave radiation) at the sea surface is so dependent on cloudiness that it is taken directly from the given NWP product (ECMWF or CORE–CNY) for use in the HYCOM. The net longwave flux is the sum of downward longwave (from the atmosphere) and upward black–body radiation. The NWP (input) black–body radiation is corrected within HYCOM to allow for the difference between NWP SST and HYCOM SST (Kara et al. 2005b). The downward longwave radiation is often not archived, but if archived, input net longwave is calculated using an archived NWP SST . Latent and sensible heat fluxes at the air–sea interface are calculated using computationally efficient bulk formulae that include the effects of dynamic stability (Kara et al. 2005d). Details of the parameterizations are given in section 3.

4. HYCOM SST Simulations

In this section , we investigate whether or not monthly mean SSTs obtained from atmospherically–forced HYCOM, which includes the effects of bulk parameterizations in its surface energy balance (see section 2), is strongly controlled by the near–surface T_a used in the atmospheric forcing. The global HYCOM simulations

presented in this paper were performed with no assimilation of any oceanic data except initialization from climatology. There is only weak relaxation to sea surface salinity to keep the evaporation–precipitation budget on track in the model. Model simulations are performed using atmospheric wind/thermal forcing from each NWP product (ERA–15, ERA–40 and CORE–CNY), separately.

Near statistical equilibrium was reached for each simulation after four model years. A linear regression analysis was performed for domain averaged quantities (layer temperature, salinity, potential and kinetic energy, etc.) to investigate statistical equilibrium in each layer, and is expressed numerically as % change per decade. The model is deemed to be in statistical equilibrium when the rate of potential energy change is acceptably small (e.g., $< 1\%$ in 5 years) in all layers. The statistical equilibrium was accomplished using climatological monthly mean thermal atmospheric forcing, but with wind forcing that includes the 6–hr sub–monthly variability because of mixed layer sensitivity to high frequency forcing (e.g., Kara et al. 2005a), a sensitivity investigated globally in section 2d.

Performing a 1–year global HYCOM simulation using any of the atmospheric forcing products required $\approx$ 15 wall–clock hours on 64 HP/Compaq SC45 processors. Thus, the $0.72°$ global HYCOM provides inexpensive, non eddy–resolving ocean model simulations.

Monthly mean SST fields obtained from the model simulations are evaluated through extensive model–data comparisons using various statistical metrics (section 4a). Within the quantitative framework, statistical error and skill analyses are then presented for quality assessment of the model in simulating climatological monthly mean SST using bulk parameterizations and the three atmospheric forcing products (section 4b).

4a. Statistical Metrics

Monthly mean HYCOM SST climatologies are constructed from SSTs obtained from the last 4 (out

of 8) model years. For example, the climatological mean January SST is formed using mean January SSTs from model years 5–8. The same process is repeated for the other months. Because all simulations performed with the 0.72° model are climatologically–forced and there are no mid–latitude mesoscale eddies, the 4–year averaging period is sufficient.

For model–data comparisons the NOAA SST climatology (Reynolds et al. 2002) is taken as a reference (truth) because its resolution (1°×1°) is close to that of HYCOM (0.72°×0.72° cos(lat)). The NOAA SST fields are mainly designed for large–scale climate studies. They are derived by a linear interpolation of the weekly optimal interpolation (OI), and use in situ and satellite SST's, making it a reliable candidate for model–data comparisons over the global ocean. The existence of the ice field in the NOAA data set is also an advantage for the model SST validation in the Arctic and Antarctic. We will also use T_a climatologies from NWP products to compare with and to evaluate the model SSTs in section 4b.

Monthly mean HYCOM SST obtained from HYCOM simulations using wind and thermal forcing from ERA–15, ERA–40 and CORE–CNY is validated using mean error (ME), root–mean–square (RMS) SST difference, correlation coefficient (R) and non-dimensional skill score (SS). Let X_i ($i = 1, 2, \cdots, 12$) be the set of monthly mean NOAA reference (observed) SST values from January to December, and let Y_i ($i = 1, 2, \cdots, 12$) be the set of corresponding HYCOM estimates at a model grid point. Also let $\overline{X}$ ($\overline{Y}$) and σ_X (σ_Y) be the mean and standard deviations of the reference (estimate) values, respectively. The statistical relationships (e.g., Murphy 1995) between NOAA and HYCOM SST time series at a given grid point are expressed as follows:

$$\text{ME} = \overline{Y} - \overline{X}, \tag{6}$$

$$\text{RMS} = \left[\frac{1}{n}\sum_{i=1}^{n}(Y_i - X_i)^2\right]^{1/2}, \tag{7}$$

17

$$R \;=\; \frac{1}{n} \sum_{i=1}^{n} (X_i - \overline{X})(Y_i - \overline{Y}) / (\sigma_X \, \sigma_Y), \tag{8}$$

$$SS \;=\; R^2 - \underbrace{[R - (\sigma_Y/\sigma_X)]^2}_{B_{\mathrm{cond}}} - \underbrace{[(\overline{Y} - \overline{X})/\sigma_X]^2}_{B_{\mathrm{uncond}}}. \tag{9}$$

ME (i.e., annual bias) is the mean error between the mean HYCOM and NOAA SST values, RMS (root–mean–square) SST difference is an absolute measure of the distance between the two time series, and the R value is a measure of the degree of linear association between the time series. The non-dimensional SS given in (9) is the fraction of variance explained by HYCOM minus two dimensionless biases (conditional bias, B_{cond}, and unconditional bias, B_{uncond}) which are not taken into account in the R formulation (8) as explained in Murphy (1988), in detail. B_{uncond}, described as systematic bias, is a measure of the difference between the means of NOAA and HYCOM SST time series. B_{cond} is a measure of the relative amplitude of the variability in the NOAA and HYCOM time series or simply a bias due to differences in standard deviations of the SST time series. Note SS is 1.0 (negative) for perfect (poor) HYCOM SST simulations.

4b. HYCOM SST Evaluation

A model validation study with respect to NOAA SST and NWP T_a from each NWP product is presented using the statistical metrics explained in section 4a. Our purpose is to determine whether or not HYCOM SST compares with the NOAA SST climatology better than T_a climatologies from each NWP product.

The original monthly mean NOAA SST climatology ($1°$) was interpolated to the global HYCOM grid ($0.72°$) for comparisons with the model SSTs. Similarly, near–surface T_a from NWP products (ERA–15, ERA–40 and CORE–CNY) is also interpolated to the model grid.

The mean HYCOM SST error, with respect to the NOAA SST climatology (Fig. 5a) and T_a climatologies (Fig. 5b) presents striking differences. In general, most of the mean errors shown in Fig. 5 do not look like

the $T_a - T_s$ fields, where T_s is the SST used by the NWP products, presented in Fig. 2 and discussed in section 3c. To better visualize whether or not HYCOM mean SST error patterns resemble T_a–SST patterns for the given re–analysis product, we calculate zonal averages of both variables (Fig. 6). Zonally–averaged T_a–SST values can also be quite different for each of these re–analysis products. It should be emphasized that HYCOM simulations using ERA–15, ERA–40 and CORE–CNY forcing have different bias values, being warmest (Table 2) with a globally averaged bias (HYCOM–NOAA SST) value of $0.57°$C for the CORE–CNY forced simulation. In general, the annual mean SST bias between HYCOM and the NOAA climatology is small ($< 0.5°$C) for all three simulations using the different atmospheric forcing products over most of global ocean.

Most importantly, there is no clear relationship between HYCOM SST bias (i.e., HYCOM SST–NOAA SST) and T_a–SST fields (Fig. 7) when using any of the atmospheric re–analysis products for forcing the ocean model. This is true despite the fact that the HYCOM SST bias and T_a–SST values from a particular re–analysis product (e.g., ERA–15) can be quite different than those from the other product (e.g., ERA–40 and CORE–CNY). If the model SST is constrained by T_a from any particular NWP product, then the differences in near–surface air temperatures between two NWP products should be similar to differences in model SSTs, obtained using the corrsponding NWP forcing in simulations. This is certainly not the case. As seen from Fig. 8, the scatter diagram of differences in T_a between ERA–40 and CORE–CNY versus those in SST from a HYCOM simulation forced with ERA–40 and CORE–CNY are quite different. While differences in T_a are generally between $0°$C and $1°$C, differences in SST are generally between $-1.5°$ to $1°$C. There is only a weak correlation ($R = -0.36$) between the two. A similar analysis for ERA–15 versus CORE–CNY is not shown because T_a from ERA–40 and ERA–15 are almost same over the global ocean.

As further evidence that bulk parameterizations are not excessively tracking T_a, the skill of monthly mean

19

model SST against monthly NOAA SST climatology and against the monthly mean re–analysis T_a (a different T_a for each simulation) is calculated (Fig. 9). The skill is much higher against observed SST than against the applied T_a over the most of global ocean. This result is especially evident in the Indian Ocean and Atlantic Ocean for the simulations using the different atmospheric forcing products. When HYCOM SST is validated against NOAA SST (NWP T_a), global average of SS values are 0.48 (0.25), 0.49 (0.15) and 0.36 (–0.14) for the ERA–15, ERA–40 and CORE–CNY forcing cases, respectively (Table 2). The reduction in SS values is generally $> 50\%$ when HYCOM SST is evaluated with respect to NPW T_a as opposed to NOAA SST. The low skill between HYCOM SST and NWP T_a is due mainly to the fact that B_{uncond} is significantly increased, i.e., there are large biases in means of HYCOM SST and NWP T_a based on the definition of unconditional bias (section 4a). Note that there is not much change in global averages of R and B_{cond}. Further comparisons of HYCOM SST versus both NOAA SST and NWP T_a clearly demonstrate that the shape of the seasonal cycle between two variables follow each other quite well as evident from R values > 0.8 (Fig. 10). The exception is the HYCOM simulation with SST compared to T_a from CORE–CNY.

Finally, overall HYCOM performance in simulating climatological SST is discussed when the model uses atmospheric forcing from ERA–15, ERA–40 and CORE–CNY. Table 2 provides a summary of statistical metrics between HYCOM SST and NOAA SST in the form of global averages. While the SST simulated by HYCOM using atmospheric forcing from CORE–CNY did not yield results as good as those using ERA–15 and ERA–40, HYCOM generally gave similar success when using any of the atmospheric forcing products.

Although there have been many improvements in the ERA–40 forcing in comparison to the ERA–15 forcing (section 2d), the model response in simulating climatological SST remains similar with global mean RMS SST differences of 0.81°C and 0.82°C, and SS values of 0.48 and 0.49 for the ERA–15 and ERA–40 cases.

There is a warm model SST bias in all of the simulations. This could be due to known shortcomings in NWP solar radiation fields, e.g., due to inaccurate cloudiness, or could result from the ocean model climatology. In any case, such a bias can be removed by applying a spatially varying but constant in time correction to the total heat fluxes (not discussed here).

5. Conclusions

The most significant result of this paper is that virtually all applications of the bulk formulae, including a fixed air temperature, does not make the sensible and latent heat behave as though the model SST tracks the near–surface air temperature too strongly. This is demonstrated using an atmospherically–forced OGCM (HYCOM) with no assimilation of any SST and no relaxation to any SST climatology.

Accurate SST simulations in an OGCM depend on how the local changes in SST made by the bulk formula are modified by vertical mixing (mixed layer physics) and advection. Atmospherically–forced HYCOM simulations without assimilation of any SST or relaxation to any SST climatology clearly reveal that while the RMS SST difference is quite small between SST and near surface air temperature over most of the global ocean, the use of the latter in a bulk parameterization does not introduce an inappropriate restoring toward observed SST in the model simulations.

Through extensive model–data comparisons using various statistical metrics, we have demonstrated that bulk parameterizations track observed SST rather than near–surface air temperature in atmospherically–forced OGCM simulations. When monthly mean SST simulated by HYCOM is compared against the monthly mean observed SST climatology from NOAA and T_a climatologies from ERA–15, ERA–40 and CORE–CNY, the model skill is higher against observed SST than against the applied T_a used in the simulations. Overall, the global mean of RMS SST difference for HYCOM is 0.81°C, 0.82°C and 0.98°C with respect to the NOAA

21

climatology over the seasonal cycle for the simulations using atmospheric wind and thermal forcing from ERA–15, ERA–40 and CORE–CNY, respectively. These global mean RMS differences increase by $\approx$ 150% (1.94°C, 2.08°C and 2.76°C, respectively) when HYCOM SST is evaluated with against near–surface air temperature from the three NWP products. Model SST validation against NOAA SST and NWP T_a yields similar correlation coefficients (generally > 0.90) over the most of global ocean, which may imply an indirect relaxation of model SST to NWP T_a. However, significantly large differences in dimensionless skill score and RMS differences between the pairs of HYCOM SST vs NOAA SST and model SST versus NWP T_a indicate that such a direct relaxation is not the case. Further, the correlation between T_a(ERA–40)–T_a(CORE–CNY) and HYCOM SST(ERA–40)–HYCOM SST(CORE–CNY) is R=–0.36 when SST relaxation to NWP near–surface air temperature would imply a substantial positive value.

Acknowledgments

APPENDIX: Latest features of HYCOM

HYCOM development has continued since the first release discussed in Bleck (2002), and new features have been added to the model. A short summary of the new improvements in the model code (version 2.1.18) is provided here.

A hybrid vertical coordinate grid generator (called hybgen) is used in choosing the optimal vertical coordinate at each location every time step. It then remaps the vertical coordinate accordingly. There are significant improvements to hybgen in the latest version of the model. The remapper in the original model assumed that each field was constant in the vertical within each layer. When remapping layers that are far from the target isopycnal, this approach can lead to excessive diffusion. The current modified remapper in HYCOM allows the profile to vary linearly across a layer if the layer is not close to being isopycnal, which significantly reduces diffusion. In such cases, the original remapper used donor–cell upwind advection, and the latest remapper uses the piecewise linear method (van Leer 1977, Lin et al. 1994) with a monotonized central–difference limiter. The hybrid grid generator and horizontal advection terms can each conserve potential temperature and salinity, potential density and salinity or potential density and potential temperature. Because the hybrid grid generator must act in density space, potential density and salinity are typically conserved in both the grid generator and advection.

Since the first release of HYCOM (Bleck 2002), there is improved support for z and σ levels in shallow water, and more flexible selection of Laplacian and biharmonic diffusion. There are several scalar advection techniques available in HYCOM, such as the donor cell, the Flux–Corrected Transport (FCT) scheme (2nd and 4th order) and Multidimensional Positive Definite Advection Transport Algorithm (MPDATA) (e.g., Smolarkiewicz and Margolin 1998; Balsara and Shu 2000). While we do not discuss it here, HYCOM simulations demonstrate that FCT is more computationally efficient and less diffusive than MPDATA, consistent with results by Smolarkiewicz (1984). Multiple tracers and off–line one–way nesting are possible in the model. HYCOM includes a hybrid to fixed vertical grid remapper, allowing fixed–coordinate nests inside hybrid coordinate outer domains. Vertical remapping uses the Piecewise Linear Method (PLM) for fixed coordinate layers. Isopycnal layer target

densities can vary spatially, and stability of these layers is controlled by locally–referenced potential density.

HYCOM can be run using any one of five mixed layer models: (1) The K–Profile Parameterization (KPP) level 1 turbulence closure (Large et al. 1997), (2) Kraus–Turner (KT) mixed layer model (Kraus and Turner 1967), (3) Price, Weller and Pinkel (PWP) mixed layer model (Price et al. 1986), (4) the Mellor–Yamada (MY) level 2.5 turbulence closure (Mellor and Yamada 1982), and (5) the NASA Goddard Institute for Space Studies (GISS) level 2 turbulence closure (Canuto et al. 2001). The model can also be run with no mixed layer model.

Earlier HYCOM simulations used the bulk parameterizations presented in Kara et al. (2002), which has a few shortcomings in the determination of exchange coefficients of sensible and latent heat fluxes (C_s and C_l) at high and low wind speeds. This was due to limitations in the observation–based input data sets used for deriving the exchange coefficients. Also, the effect of humidity was not included in the parameterizations of air–sea stability. With the availability of the improved COARE algorithm version 3.0 (Fairall et al. 2003), Kara et al. (2005d) derived new polynomials for C_l and C_s for use in HYCOM, including the full effect of stability for a wide range of conditions occurring over the global ocean. The new data set from COARE 3.0 reduces the underestimation or overestimation in the polynomials (≈ 10 to 20%) used for deriving the exchange coefficients presented in Kara et al. (2000; 2002). In addition, they have the advantage of providing reliable transfer coefficients at low and high wind speeds. They represent only an approximation to the COARE algorithm, but with the advantage of robustness and computational efficiency that make it suitable for use in various air–sea interaction applications and in any OGCM.

References

Alexander, M. A., and J. D. Scott, 1997: Surface flux variability over the North Pacific and North Atlantic Oceans. *J. Climate*, **10**, 2963–2978.

Balsara, D. S., and C.–W. Shu, 2000: Monotonicity preserving weighed essentially non–oscillatory schemes with increasingly high order of accuracy. *J. Comp. Phys.*, **160**, 405–452.

Bleck, R., 2002: An oceanic general circulation model framed in hybrid isopycnic–cartesian coordinates. *Ocean Modelling*, **4**, 55–88.

——, and S. Sun, 2004: Diagnostics of the oceanic thermohaline circulation in a coupled climate model. *Global and Planetary Change*, **40**, 233–248.

Barnier B., L. Siefridt, and P. Marchesiello, 1995: Surface thermal boundary condition for a global ocean circulation model from a three–year climatology of ECMWF analyses. *J. Marine Sys.*, **6**, 363–380.

Barron, C. N., and L. F. Smedstad, 2002: Global river inflow within the Navy Coastal Ocean Model. Proc. to Oceans 2002 MTS/IEEE Conference, 29–31 October 2002, 1472–1479.

Canuto, V. M., A. Howard, Y. Cheng, and M. S. Dubovikov, 2002: Ocean turbulence, Part II: vertical diffusivities of momentum, heat, salt, mass, and passive scalars. *J. Phys. Oceanogr.*, **32**, 240–264.

Chassignet, E. P., L. T. Smith, G. R. Halliwell Jr., and R. Bleck, 2003: North Atlantic simulations with the HYbrid Coordinate Ocean Model (HYCOM): Impact of the vertical coordinate choice, reference pressure, and thermobaricity. *J. Phys. Oceanogr.*, **33**, 2504–2526.

da Silva, A. M., C. C. Young–Molling, and S. Levitus, 1994: Atlas of Surface Marine Data 1994, Supplement B: Procedures for $1/2° \times 1/2°$ data set. NOAA Atlas NESDIS 17, U.S. Dept. of Commerce, Washington, D.C., 83 pp.

DeCosmo, J., K. B. Katsaros, S. D. Smith, R. J. Anderson, W. A. Oast, K. Bumke, and H. Chadwick, 1996: Air–sea exchange of water vapor and sensible heat: The Humidity Exchange Over the Sea (HEXOS) results. *J. Geophys. Res.*, **101**, 12 001–12 016.

Fairall, C. W., E. F. Bradley, J. E. Hare, A. A. Grachev, and J. B. Edson, 2003: Bulk parameterization of air–sea fluxes: Updates and verification for the COARE algorithm. *J. Climate*, **16**, 571–591.

Garratt, J. R., A. J. Prata, L. D. Rotstayn, B. J. McAvaney, and S. Cusack, 1998: The surface radiation budget over oceans and continents. *J. Climate*, **11**, 1951–1968.

Gibson, J. K., P. Kållberg, S. Uppala, A. Hernandez, A. Nomura, and E. Serrano, 1999: ECMWF Re–Analysis Project Report Series: 1. ERA description (Version 2), 74 pp. [Available from ECMWF, Shinfield Park, Reading, RG2 9AX, UK.]

Gill, A. E., 1982: *Atmosphere–Ocean Dynamics.* Academic Press, San Diego, CA, 662 pp

Gleckler, P. J., and B. C. Weare, 1997: Uncertainties in global ocean surface heat flux climatologies derived from ship observations. *J. Climate*, **10**, 2764–2781.

Halliwell, G. R. Jr., 2004: Evaluation of vertical coordinate and vertical mixing algorithms in the HYbrid Coordinate Ocean Model (HYCOM). *Ocean Modelling*, **7**, 285–322.

Han, Y. J., 1984: A numerical world ocean general circulation model. Part I: Basic design and barotropic experiment. *Dyn. Atmos. Oceans*, **8**, 107–140.

Han, W., P. J. Webster, R. Lukas, P. Hacker, and A. Hu, 2004: Impact of atmospheric intraseasonal variability in the Indian Ocean: low–frequency rectification in equatorial surface current and transport. *J. Phys. Oceanogr.*, **34**, 1350–1372.

Haney, R. L., 1971: Surface thermal boundary conditions for ocean circulation models. *J. Phys. Oceanogr.*, **1**,

241–248.

Hughes, T. M. C., and A. J. Weaver, 1996: Sea surface temperature–evaporation feedback on the ocean's thermohaline circulation. *J. Phys. Oceanogr.*, **26**, 644–654.

Hurlburt, H. E., A. J. Wallcraft, W. J. Schmitz Jr., P. J. Hogan, and E. J. Metzger, 1996: Dynamics of the Kuroshio/Oyashio current system using eddy–resolving models of the North Pacific Ocean. *J. Geophys. Res.*, **101**, 941–976.

Kållberg, P., A. Simmons, S. Uppala, and M. Fuentes, 2004: ERA-40 Project Report Series, **17**, the ERA–40 archive, 31 pp.

Kalnay, E., and 21 coauthors, 1996: The NCEP/NCAR 40–year Reanalysis Project. *Bull. Amer. Meteor. Soc.*, **77**, 437–471.

Kanamitsu, M., W. Ebisuzaki, J. Woollen, S.–K. Yang, J. J. Hnilo, M. Fiorino, and G. L. Potter, 2002: NCEP–DOE AMIP–II Reanalysis (R–2). *Bull. Amer. Meteor. Soc.*, **83**, 1631–1643.

Kara, A. B., H. E. Hurlburt, and P. A. Rochford, 2000: Efficient and accurate bulk parameterizations of air–sea fluxes for use in general circulation models. *J. Atmos. Oceanic Technol.*, **17**, 1421–1438.

——, ——, and ——, 2002: Air–sea flux estimates and the 1997–1998 ENSO event. *Bound.–Layer Meteor.*, **103**, 439–458.

——, A. J. Wallcraft, and H. E. Hurlburt, 2003: Climatological SST and MLD simulations from NLOM with an embedded mixed layer. *J. Atmos. Oceanic Technol.*, **20**, 1616–1632.

——, H. E. Hurlburt, P. A. Rochford, and J. J. O'Brien, 2004: The impact of water turbidity on the interannual sea surface temperature simulations in a layered global ocean model. *J. Phys. Oceanogr.*, **34**, 345–359.

——, A. J. Wallcraft, and H. E. Hurlburt, 2005a: A new solar radiation penetration scheme for use in ocean

mixed layer studies: An application to the Black Sea using a fine resolution HYbrid Coordinate Ocean Model (HYCOM). *J. Phys. Oceanogr.*, **35**, 13–32.

——, ——, and ——, 2005b: Sea surface temperature sensitivity to water turbidity from simulations of the turbid Black Sea using HYCOM. *J. Phys. Oceanogr.*, *35*, 33–54.

——, ——, and ——, 2005c: How does solar attenuation depth affect the ocean mixed layer? Water turbidity and atmospheric forcing impacts on the simulation of seasonal mixed layer variability in the turbid Black Sea. *J. Climate*, **18**, 389–409.

——, H. E. Hurlburt, and A. J. Wallcraft, 2005d: Stability–dependent exchange coefficients for air–sea fluxes. *J. Atmos. Oceanic Technol.*, **22**, 1077–1091.

Killworth, P. D., D. A. Smeed, and A. J. G. Nurser, 2000: The effects on ocean models of relaxation toward observation at the surface. *J. Phys. Oceanogr.*, **30**, 160–174.

Kraus, E. B., and J. S. Turner, 1967: A one–dimensional model of the seasonal thermocline: II. The general theory and its consequences. *Tellus*, **19**, 98–106.

Large, W. G., and S. Pond, 1981: Open ocean flux measurements in moderate to strong winds. *J. Phys. Oceanogr.*, **11**, 324–336.

Large, W. G., G. Danabasoglu, S. C. Doney, and J. C. McWilliams, 1997: Sensitivity to surface forcing and boundary layer mixing in a global ocean model: annual–mean climatology. *J. Phys. Oceanogr.*, **27**, 2418–2447.

——, and S. Yeager, 2004: Diurnal to decadal global forcing for ocean and sea–ice models: the data sets and flux climatologies. NCAR Technical Note: NCAR/TN–460+STR. CGD Division of NCAR.

Lee, S.–K., D. B. Enfield, and C. Wang, 2005: OGCM sensitivity experiments on the annual cycle of Western

Hemisphere Warm Pool. *J. Geophys. Res.*, in press.

Lin, S.–J., W. C. Chao, Y. C. Sud, and G. K. Walker, 1994: A class of the van Leer–type transport schemes and its application to the moisture transport in a general circulation model. *Mon. Wea. Rev.*, **122**, 1575–1593.

Maltrud, M. E., R. D. Smith, A. J. Semtner, and R. C. Malone, 1998: Global eddy–resolving ocean simulations driven by 1985–1995 atmospheric winds. *J. Geophys. Res.*, **103**, 30 825–30 853.

Mellor, G. L., and T. Yamada, 1982: Development of a turbulence closure model for geophysical fluid problems. *Rev. Geophys. Space Phys.*, **20**, 851–875, 1982.

Moore, A. M., and C. J. C. Reason, 1993: The response of a global ocean circulation model to climatological surface boundary conditions on temperature and salinity. *J. Phys. Oceanogr.*, **23**, 300–328.

Steele, M., R. Morley, and W. Ermold, 2001: PHC: A global ocean hydrography with a high quality Arctic Ocean. *J. Climate*, **14**, 2079–2087.

Murphy, A. H., 1988: Skill scores based on the mean square error and their relationships to the correlation coefficient. *Mon. Wea. Rev.*, **116**, 2417–2424.

——, 1995: The coefficients of correlation and determination as measures of performance in forecast verification. *Wea. Forecasting*, **10**, 681–688.

NAVOCEANO, 2003: Database description for the generalized digital environmental model (GDEM–V) Version 3.0. OAML–DBD–72, 34 pp. [Available from NAVOCEANO Oceanographic Data Bases Division, Stennis Space Center, MS 39522–5001.]

Paeth, H., M. Latif, and A. Hense, 2003: Global SST influence on the 20th century NAO variability. *Climate Dyn.* **21**, 63–75.

Paiva, A. M., and E. P. Chassignet, 2001: The impact of surface flux parameterizations on the modeling of the

North Atlantic Ocean. *J. Phys. Oceanogr.*, **31**, 1860–1879.

Perry, G. D., P. B. Duffy, and N. L. Miller, 1996: An extended data set of river discharges for validation of general circulation models. *J. Geophys. Res.*, **101**, 21 339–21 349.

Price, J. F., R. A. Weller, and R. Pinkel, 1986: Diurnal cycling: Observations and models of the upper ocean response to diurnal heating, cooling, and wind mixing. *J. Geophys. Res.*, **91**, 8411–8427.

Reynolds, R. W., N. A. Rayner, T. M. Smith, and D. C. Stokes, 2002: An improved in–situ and satellite SST analysis for climate. *J. Climate*, **15**, 1609–1625.

Rosmond, T. E., T. João , M. Peng, T. F. Hogan, and R. Pauley, 2002: Navy Operational Global Atmospheric Prediction System (NOGAPS): Forcing for ocean models. *Oceanography*, **15**, 99–108.

Schopf, P. S., and A. Loughe, 1995: A reduced–gravity isopycnal ocean model: Hindcasts of El Niño. *Mon. Wea. Rev.*, **123**, 2839–2863.

Shaji, C., C. Wang, G. R. Halliwell, Jr., and A. J. Wallcraft, 2005: Simulation of tropical Pacific and Atlantic Oceans using a hybrid coordinate ocean model. *Ocean Modelling*, **9**, 253–282.

Shriver, J. F., H. E. Hurlburt, O. M. Smedstad, A. J. Wallcraft, and R. C. Rhodes, 2006: $1/32^\circ$ real–time global ocean prediction and value–added over $1/16^\circ$ resolution. *J. Mar. Sys.*, in press.

Smedstad, O. M., H. E. Hurlburt, E. J. Metzger, R. C. Rhodes, J. F. Shriver, A. J. Wallcraft, and A. B. Kara, 2003: An operational eddy–resolving $1/16^\circ$ global ocean nowcast/forecast system. *J. Mar. Sys.*, **40–41**, 341–361.

Smolarkiewicz, P. K., 1984: A fully multidimensional positive definite advection transport algorithm with implicit diffusion. *J. Comput. Phys.*, **54**, 325–362.

——, and L. J. Margolin, 1998: MPDATA: A finite difference solver for geophysical flows. *J. Comp. Phys.*,

140 459–480.

Sun, S., and J. Hansen, 2003: Climate simulations for 1951–2050 with a coupled atmosphere–ocean model. *J. Climate*, **16**, 2807–2826.

Thacker, W. C., S.–K. Lee, and G. R. Halliwell, Jr., 2004: Assimilating 20 years of Atlantic XBT data into HYCOM: a first look. *Ocean Modelling*, **7**, 183–210.

van Leer, B., 1977: Towards the ultimate conservative difference scheme IV. A new approach to numerical convection. *J. Comp. Phys.*, **23**, 276–299.

Wallcraft, A. J., Kara, A. B., Hurlburt, H. E., and P. A. Rochford, 2003. The NRL Layered Global Ocean Model (NLOM) with an embedded mixed layer sub–model: Formulation and tuning. *J. Atmos. Oceanic Technol.*, **20**, 1601–1615.

FIGURE CAPTIONS

FIG 1. Grid intervals in the 0.72° global HYCOM: (a) Zonal (longitudinal) grid interval, ranging from a minimum of 17 km to a maximum of 80 km over the global ocean, (b) Meridional (latitudinal) grid interval, ranging from a mimimum of 17 km to 79 km over the global ocean, (c) the ratio of zonal to meridional grid, and (d) the same as (c) but with the color bar designed only to show regions where the zonal grid interval is longer or shorter than meridional one over the global ocean.

FIG. 2. Climatological mean of the difference between near–surface air temperature (T_a) and sea surface temperature (i.e., T_a–T_s) over the global ocean. Both T_a and T_s fields from COADS, ERA–15, ERA–40 and CORE–CNY are interpolated to the 0.72° HYCOM grid, and the difference between the two is formed at each grid point.

FIG. 3. Scatter plots of T_a versus T_s based on annual mean values, each at 1° bins over the global ocean. Both T_a and T_s fields are from COADS, ERA–15, ERA–40 and CORE–CNY, respectively.

FIG. 4. Scatter plots of near–surface air temperature (T_a) versus T_a–T_s based on annual mean values (see Fig. 2), each at 1° bins over the global ocean.

FIG. 5. (a) Annual mean error (bias) obtained from HYCOM simulations using climatological atmo-spheric forcing from ERA–15, ERA–40 and CORE–CNY, when the model SST is compared to (a) NOAA SST climatology and (b) near–surface air temperature climatology from each NWP product. Atmospherically–forced HYCOM simulations include no assimilation of any SST or air temperature. In the model simulations, there is no relaxation to any SST or air temperature climatology. We evaluate time series of HYCOM SST versus NOAA SST (similarly HYCOM SST versus NWP T_a) climatologies from January to December at each model grid point, producing the annual mean bias maps over the global ocean. In the maps, the white color represents

bias values between -0.25°C and 0.25°C.

FIG. 6. Zonal averages of mean error between HYCOM and the NOAA SST climatology when the model uses climatological atmospheric forcing (wind and thermal forcing) from the three NWP products: ERA–15, ERA–40 and CORE–CNY. Also included are zonal averages of T_a–SST for each product. Zonal averages are calculated at each 1° latitude belt over the global ocean.

FIG. 7. Scatter plots for HYCOM SST bias (HYCOM SST–NOAA SST) versus T_a–SST based on zonally–averaged values shown in Fig. 6. The least square line for each product is also shown along with the linear R value between the two variables for each product, respectively. The least squares lines are based on zonally–averaged values for each NWP product. Zonally–averaged values are used for plotting purposes to reduce number of data over the global ocean. The regions where ice is located are not used in the analyses.

FIG. 8. Scatter plots for SST differences from two HYCOM simulations forced with ERA–40 and CORE–CNY versus differences in T_a between ERA–40 and CORE–CNY. Results are based on annual mean values over the global ocean except ice–covered regions. The least squares line having a linear R value of –0.36 is also shown.

FIG. 9. Dimensionless skill score calculated over the seasonal cycle for HYCOM SST with respect to (a) NOAA SST climatology and (b) near–surface air temperature climatology from each NWP product. Results are shown when the model is forced with NWP products (ERA–15, ERA–40 and CORE–CNY), separately. Note that air temperature climatology used for comparisons in (b) is different for each panel. As in Fig. 5, atmospherically–forced HYCOM simulations include no assimilation of any SST or air temperature, also no relaxation to any SST or air temperature climatology. We evaluate time series of HYCOM SST versus NOAA SST (similarly HYCOM SST versus NWP air temperature) climatologies from January to December at each
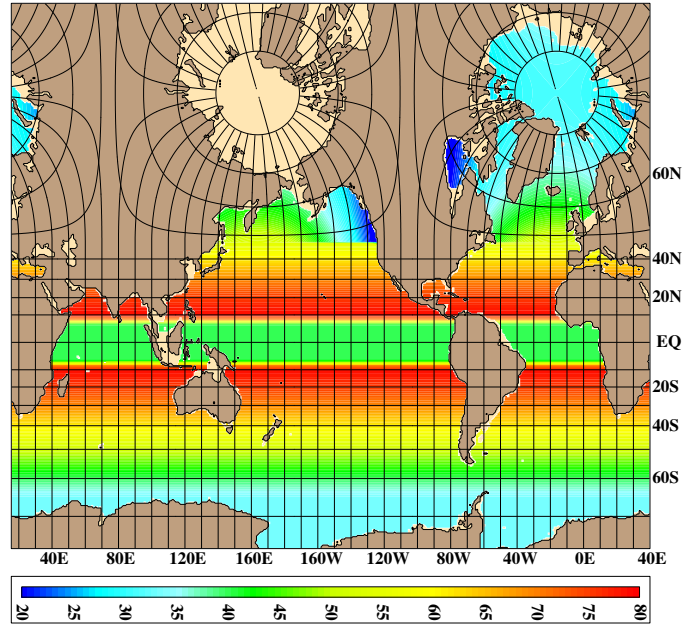
model grid point, producing the skill score maps over the global ocean. In the maps, blue (red) color shows negative (positive) skill scores, and white color denotes skill score values close to 0.

FIG. 10. The same as Fig. 9 but for the correlation coefficient. In the maps, the white color represents correlation values of > 0.95.
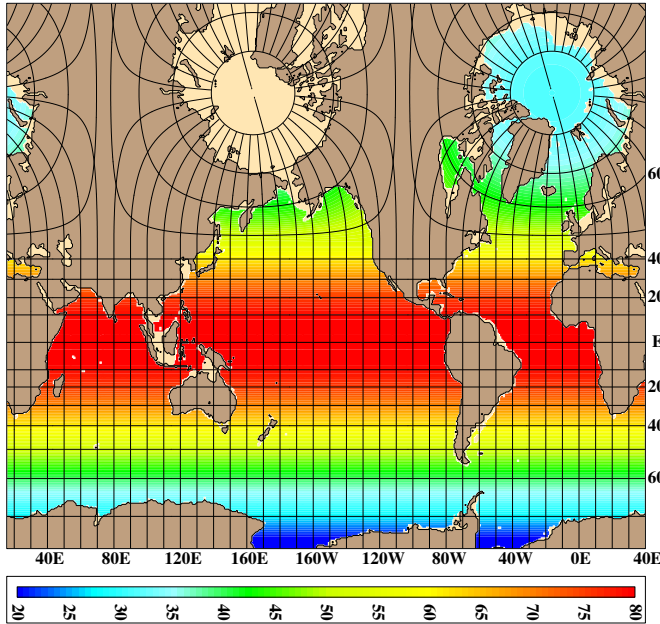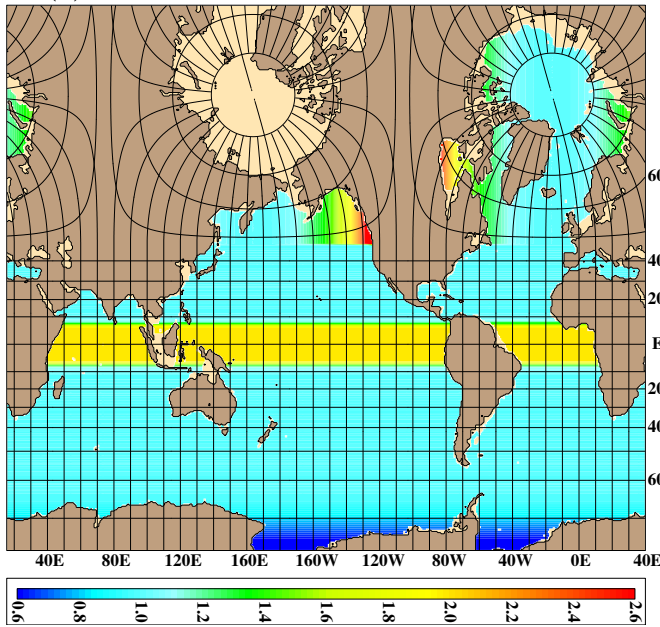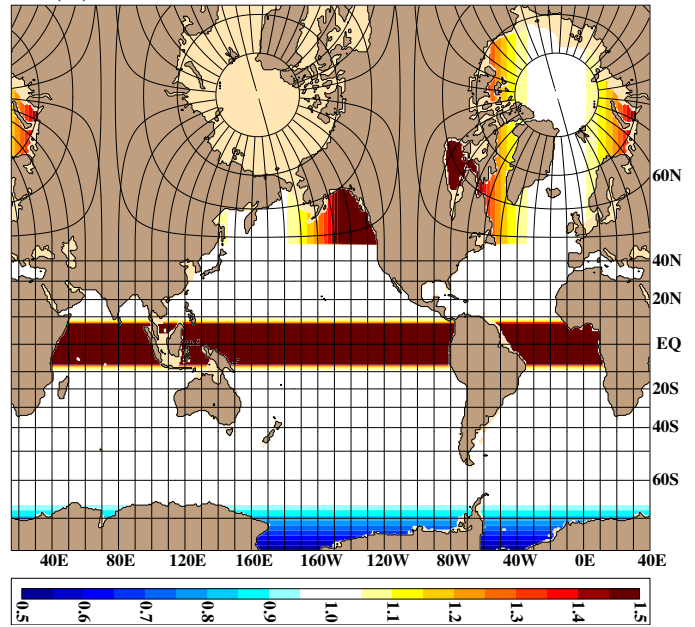
Figure 1: Grid intervals in the 0.72° global HYCOM: (a) Zonal (longitudinal) grid interval, ranging from a minimum of 17 km to a maximum of 80 km over the global ocean, (b) Meridional (latitudinal) grid interval, ranging from a mimimum of 17 km to 79 km over the global ocean, (c) the ratio of zonal to meridional grid, and (d) the same as (c) but with the color bar designed only to show regions where the zonal grid interval is longer or shorter than meridional one over the global ocean.
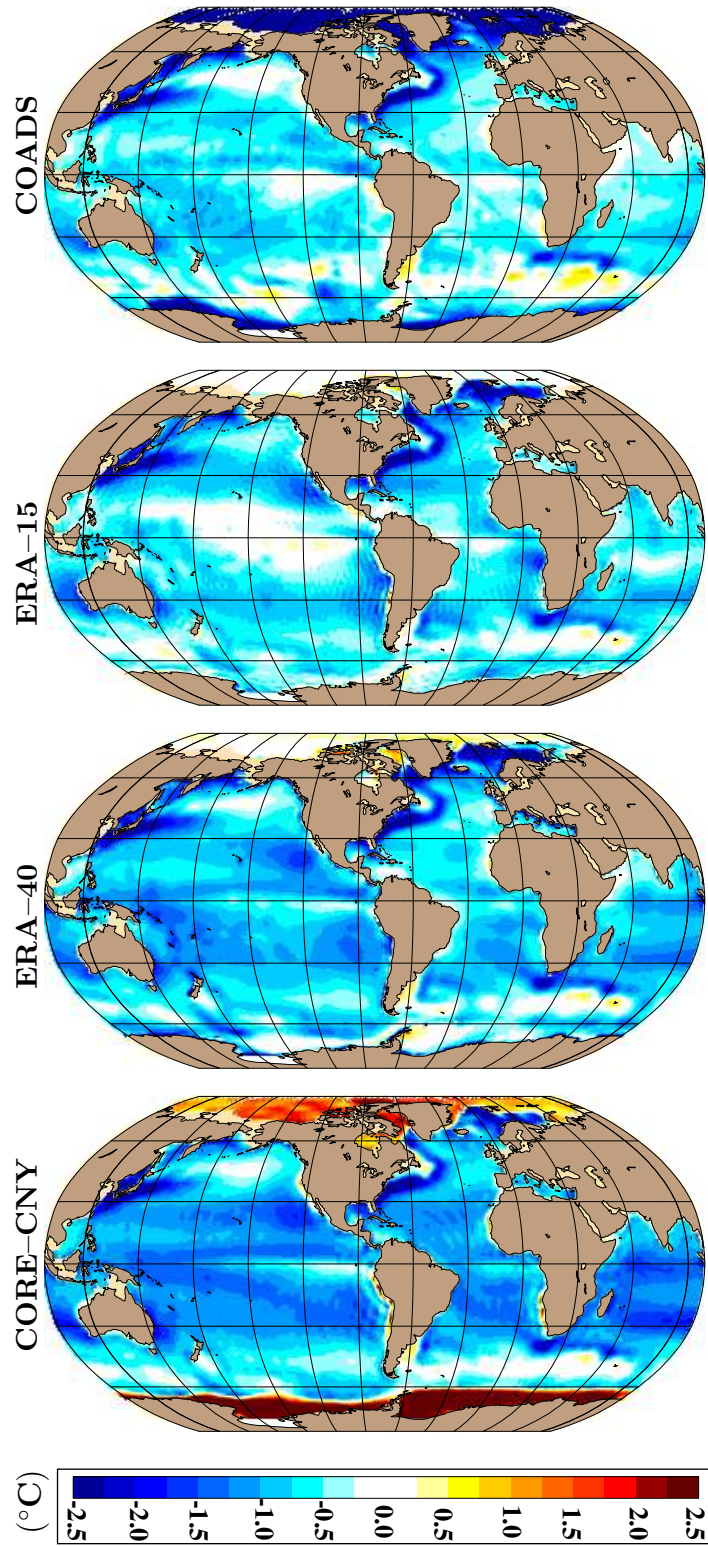
Climatological mean bias: $T_a - T_s$

Figure 2: Climatological mean of the difference between near–surface air temperature (T_a) and sea surface temperature (i.e., T_a–T_s) over the global ocean. Both T_a and T_s fields from COADS, ERA–15, ERA–40 and CORE–CNY are interpolated to the 0.72° HYCOM grid, and the difference between the two is formed at each grid point.
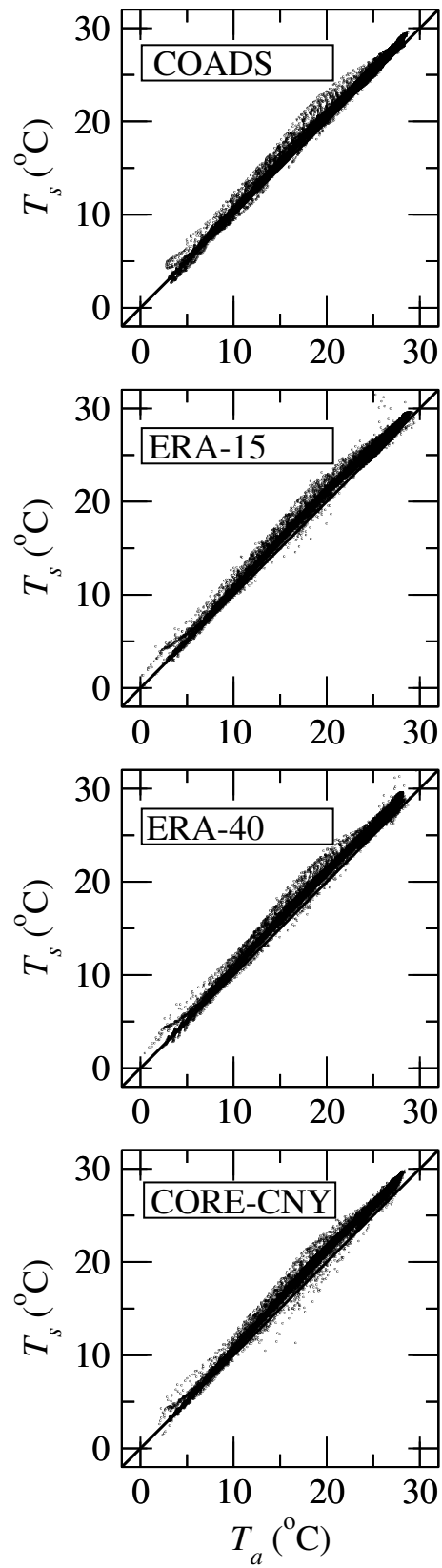
Figure 3: Scatter plots of T_a versus T_s based on annual mean values, each at $1°$ bins over the global ocean. Both T_a and T_s fields are from COADS, ERA–15, ERA–40 and CORE–CNY, respectively.
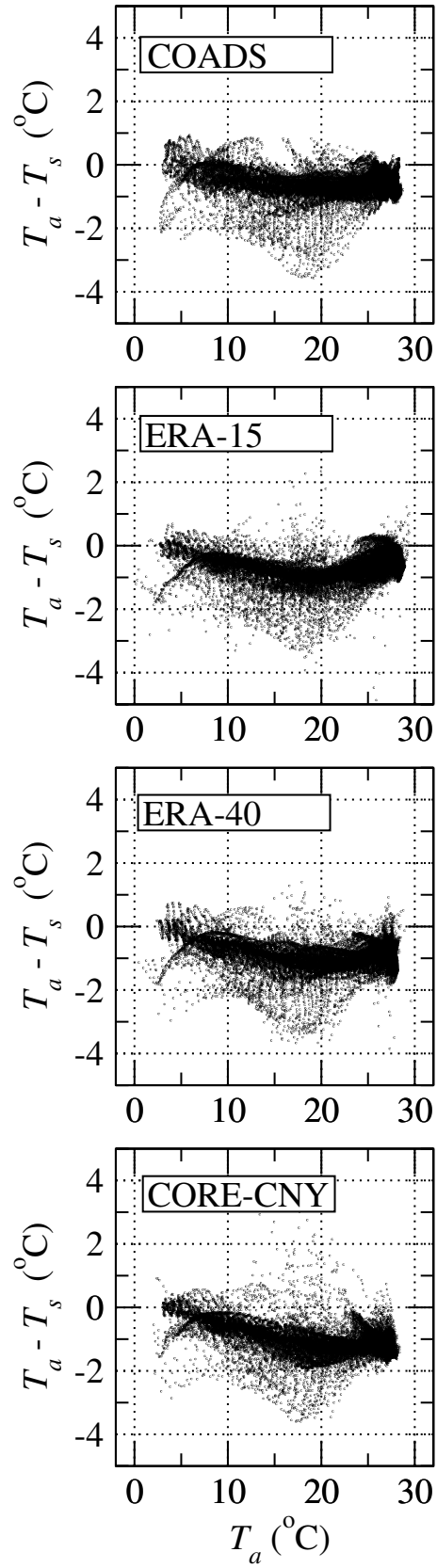
Figure 4: Scatter plots of near–surface air temperature (T_a) versus T_a–T_s based on annual mean values (see Fig. 2), each at 1° bins over the global ocean.

(a) Bias: HYCOM SST − NOAA SST   **(b) Bias: HYCOM SST − NWP T_a**

ERA–15

ERA–40

CORE–CNY

(°C) -2.5 -2.0 -1.5 -1.0 -0.5 0.0 0.5 1.0 1.5 2.0 2.5

Figure 5: (a) Annual mean error (bias) obtained from HYCOM simulations using climatological atmospheric forcing from ERA–15, ERA–40 and CORE–CNY, when the model SST is compared to (a) NOAA SST climatology and (b) near–surface air temperature climatology from each NWP product. Atmospherically–forced HYCOM simulations include no assimilation of any SST or air temperature. In the model simulations, there is no relaxation to any SST or air temperature climatology. We evaluate time series of HYCOM SST versus NOAA SST (similarly HYCOM SST versus NWP T_a) climatologies from January to December at each model grid point, producing the annual mean bias maps over the global ocean. In the maps, the white color represents bias values between −0.25°C and 0.25°C.
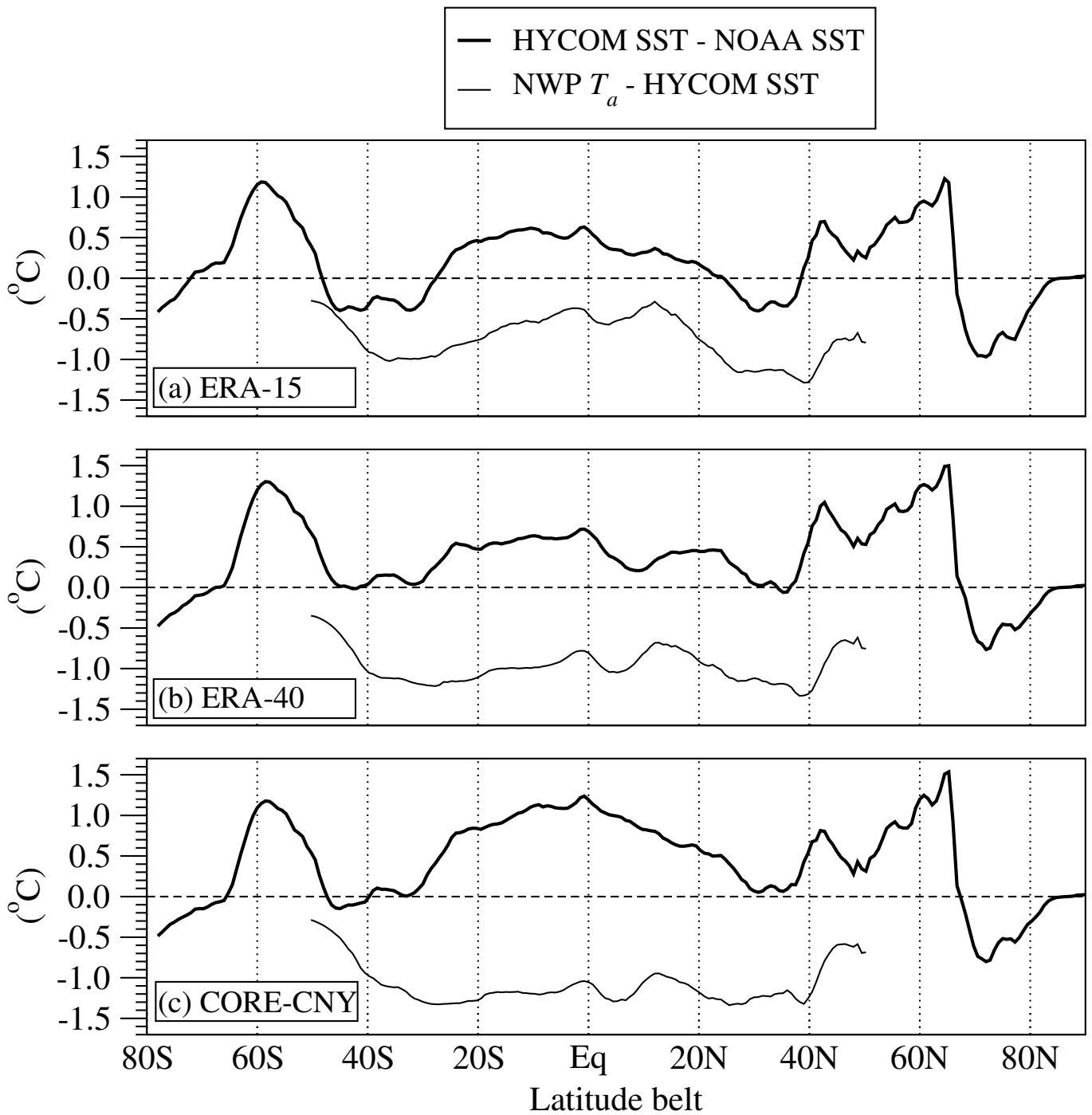
Figure 6: Zonal averages of mean error between HYCOM and the NOAA SST climatology when the model uses climatological atmospheric forcing (wind and thermal forcing) from the three NWP products: ERA–15, ERA–40 and CORE–CNY. Also included are zonal averages of T_a–SST for each product. Zonal averages are calculated at each 1° latitude belt over the global ocean.
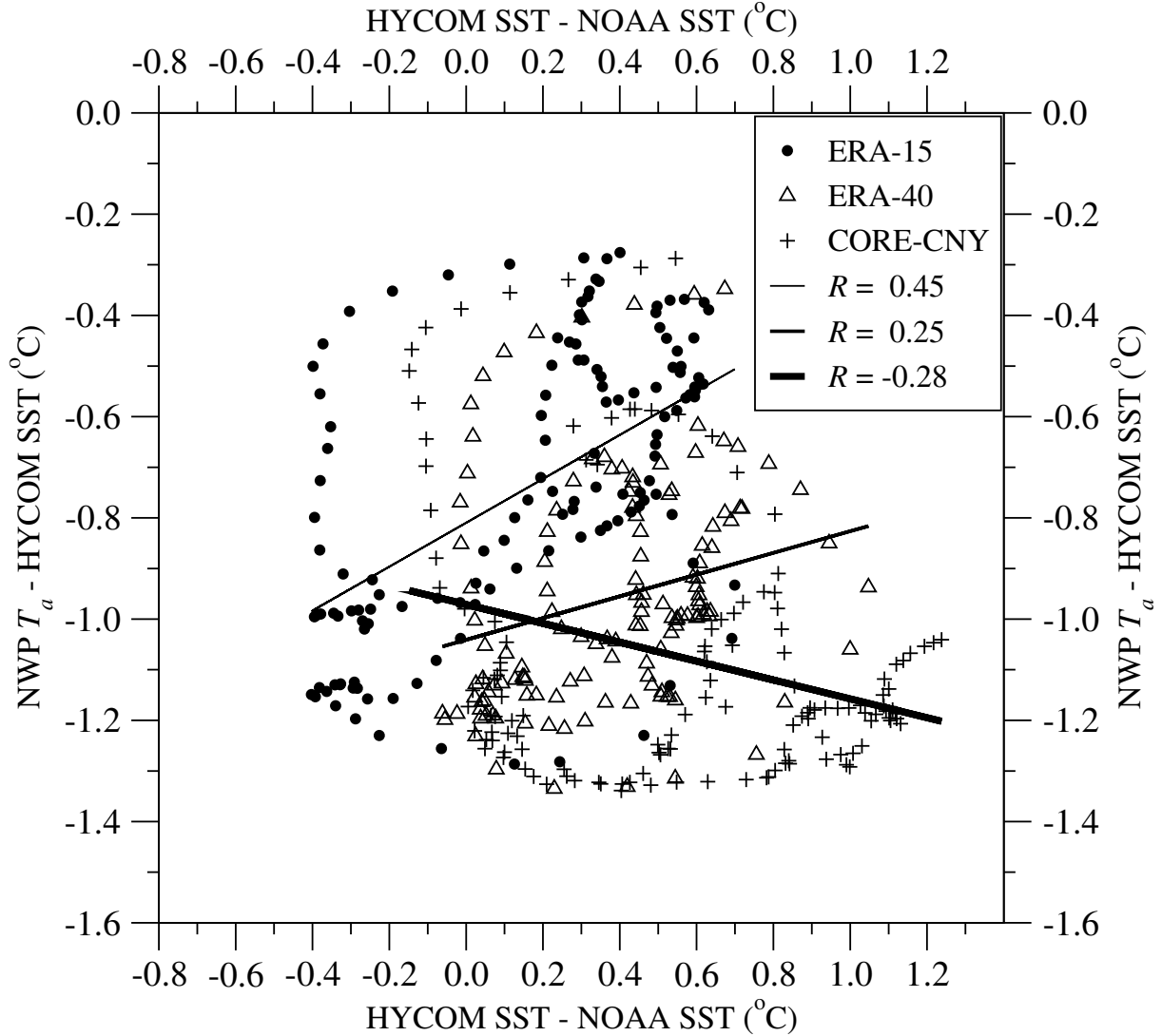
Figure 7: Scatter plots for HYCOM SST bias (HYCOM SST–NOAA SST) versus T_a–SST based on zonally–averaged values shown in Fig. 6. The least square line for each product is also shown along with the linear R value between the two variables for each product, respectively. The least squares lines are based on zonally–averaged values for each NWP product. Zonally–averaged values are used for plotting purposes to reduce number of data over the global ocean. The regions where ice is located are not used in the analyses.
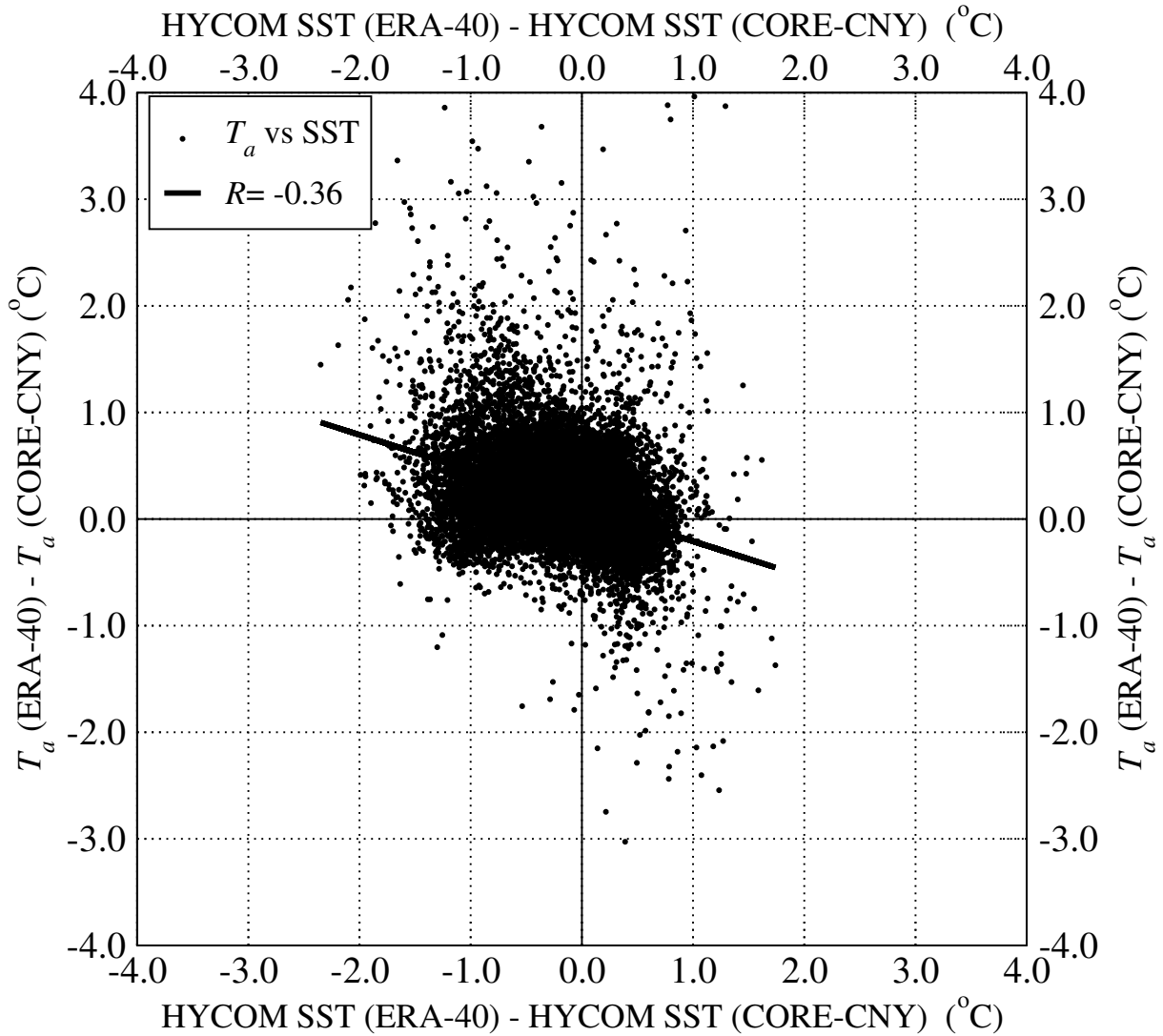
Figure 8: Scatter plots for SST differences from two HYCOM simulations forced with ERA–40 and CORE–CNY versus differences in T_a between ERA–40 and CORE–CNY. Results are based on annual mean values over the global ocean except ice–covered regions. The least squares line having a linear R value of –0.36 is also shown.

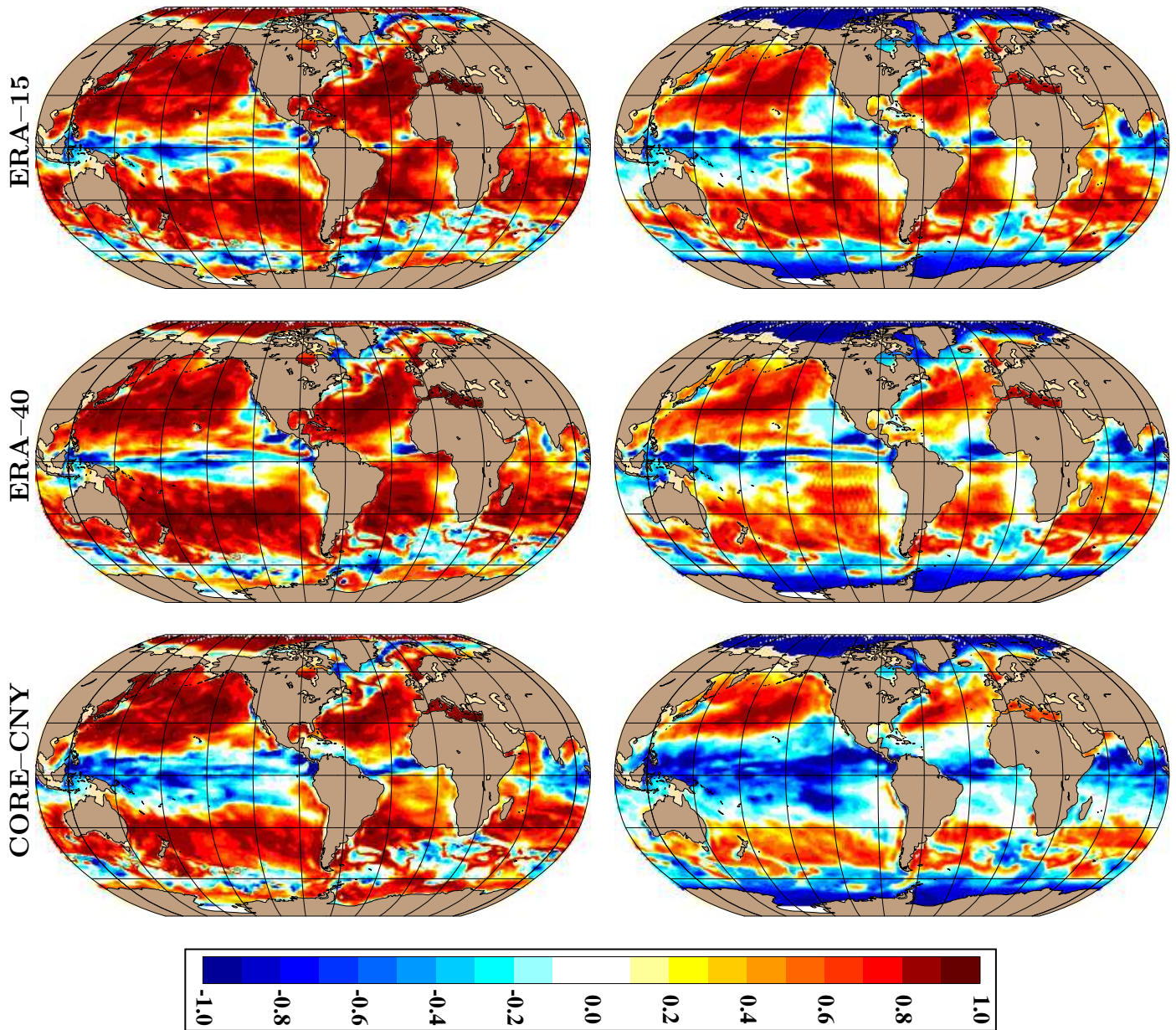**(a) Skill: HYCOM vs NOAA SST**   **(b) Skill: HYCOM SST vs NWP T_a**

Figure 9: Dimensionless skill score calculated over the seasonal cycle for HYCOM SST with respect to (a) NOAA SST climatology and (b) near–surface air temperature climatology from each NWP product. Results are shown when the model is forced with NWP products (ERA–15, ERA–40 and CORE–CNY), separately. Note that air temperature climatology used for comparisons in (b) is different for each panel. As in Fig. 5, atmospherically–forced HYCOM simulations include no assimilation of any SST or air temperature, also no relaxation to any SST or air temperature climatology. We evaluate time series of HYCOM SST versus NOAA SST (similarly HYCOM SST versus NWP air temperature) climatologies from January to December at each model grid point, producing the skill score maps over the global ocean. In the maps, blue (red) color shows negative (positive) skill scores, and white color denotes skill score values close to 0.

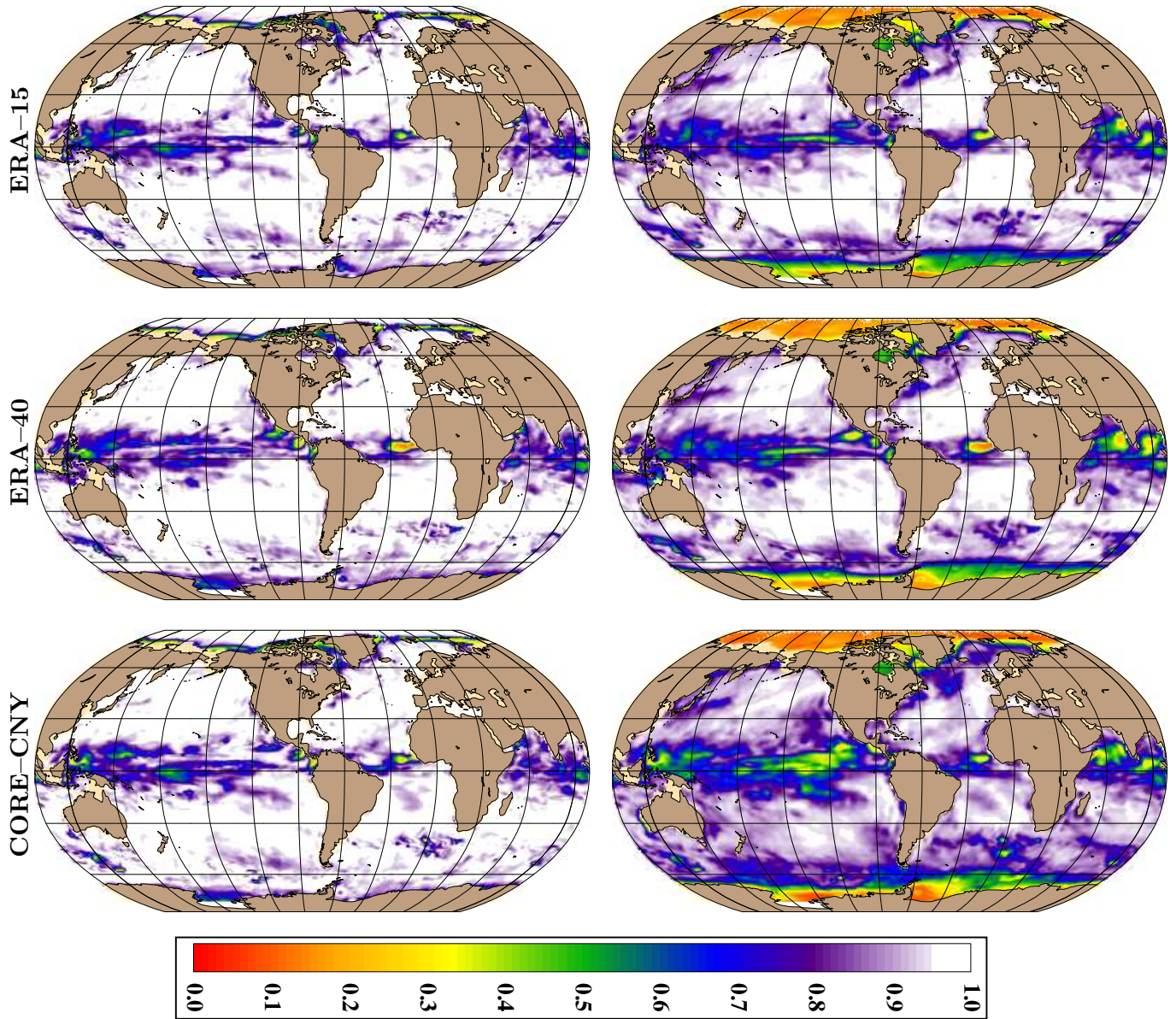**(a) Correlation: HYCOM vs NOAA SST**   **(b) Correlation: HYCOM SST vs NWP T_a**

Figure 10: The same as Fig. 9 but for the correlation coefficient. In the maps, the white color represents correlation values of > 0.95.

Table 1: Global averages for near–surface air temperature (T_a), T_s and difference between the two from the observational–based COADS data set and three NWP–based products. Further information about COADS, ERA–15, ERA–40 and CORE–CNY can be found online at several web sites. For example, as of this writing, web addresses are http://iridl.ldeo.columbia.edu/SOURCES/.DASILVA/.SMD94 for COADS, http://badc.nerc.ac.uk/data/ecmwf-era/ERA.html for ERA–15, http://badc.nerc.ac.uk/data/ecmwf-e40/e40_background_html for ERA–40, and http://data1.gfdl.noaa.gov/nomads/forms/mom4/CORE/CNYF_1p0.html for CORE–CNY. The web addresses may be subject to changes by the originators. All the NWP products have different boundary layer parameterizations, physics, data assimilation methods and different satellite data used in the assimilations. Therefore, differences in their output variables are expected.

Data	T_a	T_s	T_a–T_s
COADS	21.4	22.0	–0.6
ERA–15	21.4	22.1	–0.7
ERA–40	21.2	22.1	–0.9
COARE–CNY	20.9	22.0	–1.1

Table 2: Global averages of statistical metrics calculated over the seasonal cycle between HYCOM and NOAA SST (see text for details). Results are given for HYCOM simulations using atmospheric forcing (wind and thermal forcing) from ERA–15, ERA–40 and CORE–CNY. Basin–averaged means are calculated over the entire ice–free global HYCOM domain. Similar comparisons are made between HYCOM SST and NWP air temperature (a different T_a for each product). A SS value of 1 indicates perfect SST match with respect to NOAA SST (or NWP T_a) climatology. All R values are statistically significant in comparison to 0.70 at a 95% confidence interval.

NOAA SST	ERA–15	ERA–40	CORE–CNY
ME (°C)	0.23	0.42	0.57
RMS (°C)	0.81	0.82	0.98
B_{cond}	0.08	0.07	0.07
B_{uncond}	0.29	0.29	0.42
R	0.92	0.92	0.92
SS	0.48	0.49	0.36
NWP T_a	ERA–15	ERA–40	CORE–CNY
ME (°C)	1.54	1.73	2.32
RMS (°C)	1.94	2.08	2.76
B_{cond}	0.05	0.05	0.07
B_{uncond}	0.46	0.54	0.73
R	0.87	0.86	0.81
SS	0.25	0.15	–0.14